Secure Palmprint Recognition based on Multispectral Sequential Capture

Amine AMRAOUI[1]*, Mounir AIT KERROUM[2], Youssef FAKHRI[3]
LaRI Laboratory-Faculty of Science, Ibn Tofail University, Kenitra, Morocco[1, 3]
LaRI Laboratory-ENCG, Ibn Tofail University, Kenitra, Morocco[2]

***Abstract*—The security of personal identities is a serious challenge in today's digital world, with so many daily transactions requiring secure solutions. The use of biometric characteristics of the person is presented as the reliable solution to solve this problem. Indeed, this solution is effective, but it hides a weak point which lies in the ability to reproduce certain biometric characteristics for fraud. To overcome this weak point, we propose a secure approach for palmprints that relies on the concept of merging multiple features. Indeed, these features will be extracted from multi-spectral images with different spectra, which allow the extraction of information under the skin of the palm for two different spectrums sequentially in two different times (T1, T2) but instantly. The instant fusion of these characteristics will be impossible to replicate. The images used are grayscale. To satisfy a construction of a reliable and secure system, for this kind of patterns (palmprints), we will use the Compound Local Binary Pattern method, since this method adds an additional bit for each P bits coded by LBP corresponding to a neighbor of the local neighborhood, in order to build a robust system. This feature descriptor, it uses both the sign and tilt information of the differences between the central and neighboring gray values. The reliability of the proposed approach has been demonstrated on the Casia Multi-Spectral database. The final experimental results show reliable recognition rates and these recognition rates vary between 99% and 100% for the left and right palms.**

***Keywords*—Biometrics; multispectral palmprint, local features; fusion; compound local binary pattern**

I. INTRODUCTION

The uniqueness of personal identity has always been the major concern of individuals in society. This concern is justifiable given the seriousness of the risks. The identity is the entity requested to ensure the majority of critical transactions. Various applications have been proposed to guarantee this uniqueness, however, in this set of applications, biometrics remains the most appropriate solution [1, 2]. A multitude of scientific research has been undertaken in recent decades in this direction. Researchers have proposed a large set of recognition systems with very promising results. A large number of modalities have been investigated and they have shown a distinctive character that ensures the uniqueness of the identity. Among these modalities, we can cite the use of the fingerprint [3], the iris [4], the finger knuckle [5], the voice [6], the hand geometry [7], etc. However, it should be noted that these different biometric mechanisms offer advantages on the one hand and disadvantages on the other. The suitability of a mechanism for all current applications cannot be judged with certainty. Because of this, scientific researchers have varied their research to try to meet the requirements of different fields. Like all these researchers, the orientation of our work has been guided by constraints. One of the most important constraints that we have taken into consideration relying on the Biometric Zephyr analysis, is intrusion [8]. Indeed, the intrusive nature of the sensors makes the participants uncomfortable during the capture process such as the retina and iris based sensors [9]. This constraint, directed us towards the use of the modalities which reduce the impact of this factor like the descriptors based on the hand. The ease of use and convenience for this kind of descriptors has pushed research in this direction. In the literature, there is a large number of studies that have opted for the use of hand-based modalities and in various fields, such as fingerprints [10, 11], hand geometry [12, 13], finger knuckle print [14, 15] and palmprints [16-18]. Nevertheless, fingerprint-based systems have many challenges that are summed up in the ability of their spoofing easily by third parties [19, 20]. Furthermore, compared to other biometric descriptors, palm prints show low distortion, good stability over time and a highly distinctive character [21, 22]. Unfortunately, palmprint patterns are sensitive to pose orientations, lighting variations, and sensor noise. These factors can lead to misclassification and therefore affect the ability of such systems to recognize users. To overcome these problems, various researches have been done on the extraction mechanisms to improve the relevance of features, which will have a positive impact on the matching of these features. The majority of these researches employed coding-based, statistics-based, subspace-based, and line-based methods.

Coding-based methods are a category widely used in much research on palmprint recognition systems. Various palmprint codes have been generated, among which we cite the fusion code [23], which allows the coding of the phases and the responses of the six Gabor filters. The Robust Line Orientation Code (RLOC) [24], which allows the extraction of palmprint orientation features with a modified finite Radon transform. The feature vector obtained in this technique is used as a competitive code. But, the extracted features have a large size, which leads to a classification over-fitting. The combination of Block Dominant Orientation Code (BDOC) for rough characteristics extraction and Block-based Histogram of Oriented Gradient (BHOG) for fine characteristics extraction [25], Half-Orientation Code (HOC) for palmprint feature extraction, this code employs half Gabor filters [26]. The Double Orientation Code (DOC) of Gabor

*Corresponding Author.

filters for feature extraction with a nonlinear classifier [27]. This category can be expensive in computation time and implementation.

Another category that is also used, this category relies on statistics-based approaches; they have shown good performance [28–29]. A multitude of statistical methods have been employed in this category such as variance, standard deviation, energy and histograms of local binary models [30], Zernike and Hu moments[31]. Some transformations have also been used such as the wavelet transform to convert the palmprint image into a small number of wavelet coefficients, and then calculate the variance and the mean of these coefficients to generate the image characteristics [32]. Other methods have been introduced to calculate the statistical characteristics after the extraction phase with certain filters and transforms such as Gaussian derivative filters, Gabor wavelet, and Fourier transform [33]. The use of principal component analysis (PCA) and wavelet transform to extract features from the quaternion matrix, combined with the Euclidean distance classifier for matching process [34].

Approaches based on the concept of subspace also form an important category that intervenes in the construction of recognition systems. This kind of approach has been widely used in scientific research related to palmprint recognition. Among this research, we can cite the use of approaches in the works such as principal component analysis (PCA) [35], independent component analysis (ICA) [36] and linear discriminant analysis (LDA) [37]. In [38], a method to convert palmprint images into a set of feature space, named eigenpalms was proposed to build a palmprint recognition system. For matching, the Euclidean distance classifier was been employed. Researchers in [39] used Two-dimensional vertical and horizontal LDA (2DLDA) to extract Gabor features and then a distance-based adaptive approach to merge the vertical and horizontal features. Other approaches based on multi-spectral images have been deployed; in [40] kernel discriminant analysis (KDA) was used to reduce feature dimensionality and classification was provided by a KNN classifier and in [41], researchers proposed a multi-spectral method based on a digital Shearlet transform. This category can be affected by environmental variables (light and pose rotation).

A last category which is based on the use of lines to recover outlines and lines of palm prints with edge detection methods. Among the studies based on this concept we can cite [42], in which a technique that employs the Sobel edge detector with morphological operations to ensure the feature extraction phase of lines and [43] who used the Sobel mask to calculate the amplitudes of the lines and projected those amplitudes along the *x* and *y* axes to produce the discriminant histograms for each class. This last category offers medium performance.

In a brief summary of what preceded, we can identify the following issues: the intrusiveness of the modality, the complexity of many methods employed, the sensitivity of some methods to environmental lighting or rotation of employed modality (in the case of the hand-based modalities) and finally the possibility of usurping the personal identity by the reproduction of false descriptors.

To overcome these problems, we propose a reliable approach using local features to build a non-intrusive, secure, robust and efficient recognition mechanism, in which, we take into account the optimization of the computational complexity. We will use palmprints to reduce intrusiveness. To reduce the influence of environment lighting, capture conditions and extract relevant features, we will use method of extracting local features Compound Local Binary Pattern (CLBP) [44, 45], which we will evaluate on different block sizes with different classifiers. The classification phase will be based on the use of classifiers that reduce computation time such as distance-based classifiers. We will test three variants of measurements: Jeffrey Divergence, City-Block and Euclidian Distance. We will also pre-process the Casia Multispectral Palmprint database [46], in order to reduce computation time and improve performance.

This paper is organized as follows: Section II describes the proposed approach and the methods used. Section III reports and discuss the experimental results conducted on the Casia Multispectral Palmprint database. Finally, Section IV draws conclusions.

II. Proposed Approach

The design of the global system went through several stages before arriving at the final system scheme. In the first part, we chose a local extraction method, given the nature of palmprints pattern, which are rich with local information. In addition, this method must be as robust to variations in the lighting of the environment and to rotations. It turns out that the compound local binary pattern method [47] can satisfy these constraints. The objectives of this part can be summarized in two points. In the first point, the goal is trying to demonstrate the reliability of the chosen extraction method.

The second point will concern the classification, which represents a crucial phase to determine the reliability of the systems and their cost in computing time. In this sense and in order to satisfy its needs, experiments will be made with distance-based classifiers, known for their reduced computation time. Several classifiers will be discussed at the beginning, then the choice will be based on the most appropriate with respect to the local extraction method used (ratio optimization: recognition rate and computation time). The concept used for this evaluation is illustrated in Fig. 1.

In the second part, a new gait will be experimented, which aims at the adequacy of the size of the cropping chosen to extract the regions of interest, in order to further improve the reliability and the reduction of the calculation times. During this last point, we will extract the regions of interest with the Principal Based ICP method [48], this cropping will be done with a size of 192x192 pixels; which will generate the first database of ROI images, thereafter, we will proceed to a resizing of the ROI images with the size 128x128 pixels to obtain the second database (Fig. 2). With this approach, it will be discovered that the size 128x128 pixels can offer better results than 192x192 pixels, this can be justified by the fact that if the size of the division block is large and the pattern is

poor in information, then the rate inter-class similarity increases, which will reduce the recognition rate. The consequence of this increase will be a reduction in system performance and an increase in computation times, which we aim to avoid with this approach.

Subsequently, in the experimental part, the relationship between cropping resolution and scoring performance will be demonstrated.

Finally, in the last part, the experimental results and the conclusions obtained in the two previous steps will be used to test the reliability and robustness of the proposed approach. In the proposed approach, the choice will be in favor for a sequential capture of two images at two different times T1 and T2, which follow each other with two different spectrums, in our case we will use the 640 nm spectrum for image 1 and 940 nm for the image (we will explain this choice in the experimental part). These two images will form two different descriptors, in addition, with the 940nm spectrum some veins under the skin will be visible and other characteristics will change. The proposed palmprint multispectral recognition system is shown in Fig. 3.

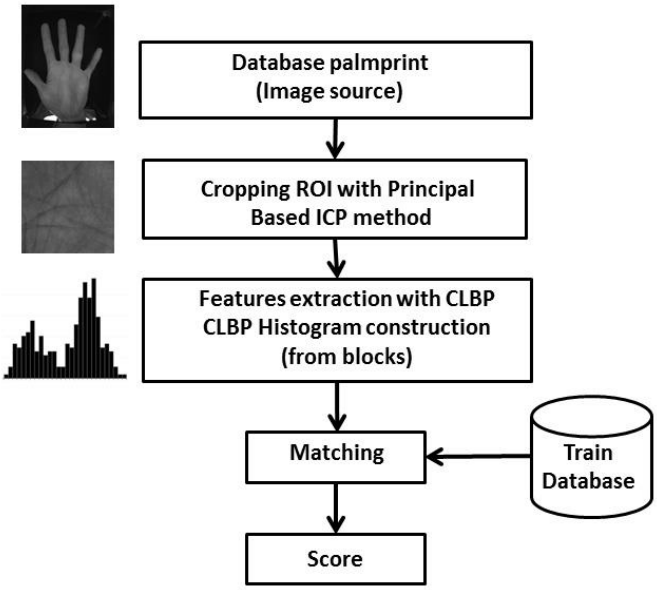

Fig. 1. FKP Recognition System adopted for evaluation.

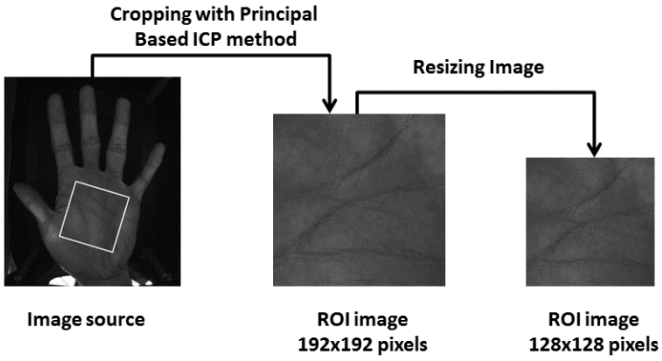

Fig. 2. Cropping and resizing process for ROI image.

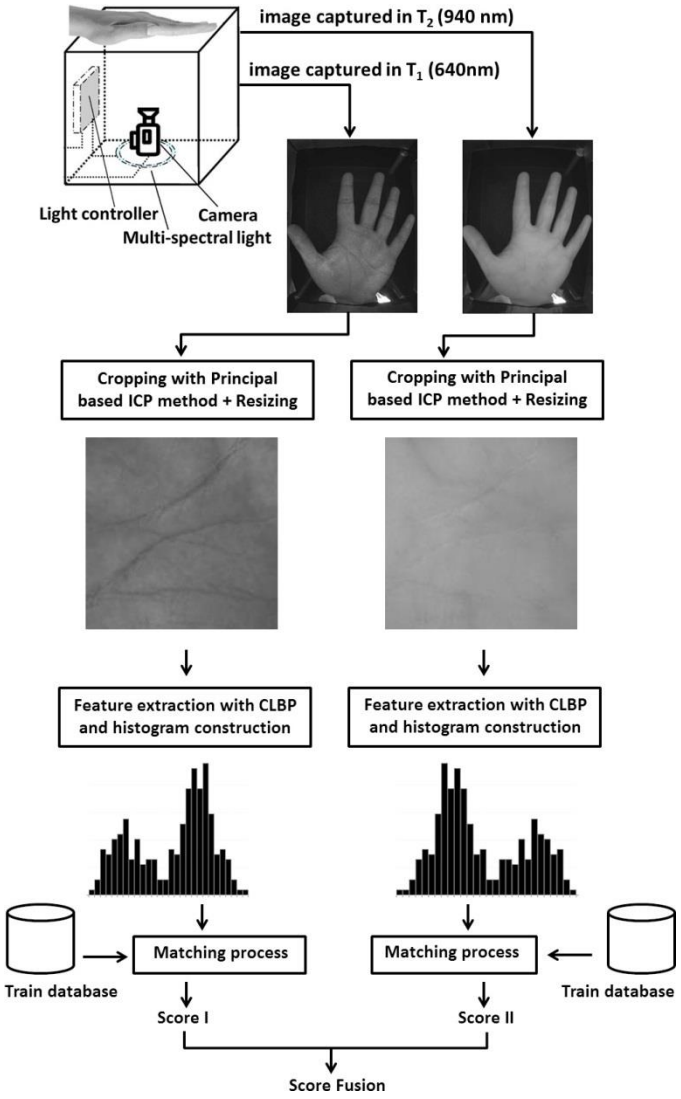

Fig. 3. The proposed multispectral recognition system.

Indeed, this sequential capture in very close times (in ms) will aim; the security of the capture phase against any attempts at fraud or use of false artifacts. Since these fake methods cannot deploy quickly to present two descriptors in a short time (in ms) and therefore, even if descriptor 1 (image1) will be spoofed, descriptor 2 (image2) will not. This will secure the proposed system. This approach will be based on fusion at the score level. The results obtained in this step will be analyzed and compared to the previous step.

A. Features Extraction Process

The construction of recognition mechanisms is generally based on two key factors; the first factor depends on the computation time allocated to satisfy the operation, the second factor depends on the efficiency and the recognition rates. It is also necessary to take into consideration the conditions of the environment which can constitute handicaps for the performance. To avoid this kind of handicaps, local methods robust to rotations and light variations will be introduced (which is the case of this database of palm prints).The feature extraction step will be ensured by a robust variant of Local

Binary Patterns (LBP), this method is called Compound Local Binary Patterns (CLBP) [47]. The LBP method was first introduced by Ojala and Al [49], this method is effective for feature extraction from images in real environments. The local binary pattern is recognized by a gray scale texture operator characterizing the local spatial structure of the image texture [50]. Given a central pixel in the image, a pattern code is calculated by comparing it to its neighbors. This method is illustrated in Fig. 4. The LBP operator calculates the signs of the differences of the gray levels of P neighbors equidistant with respect to the central pixel, which will be represented with a binary number of P bits (Fig. 4). If a neighbor is not exactly on a pixel position, then the value of that neighbor will be estimated using bilinear interpolation. The histogram of the coded image block obtained with the LBP operator will then be used as a texture descriptor for this block.

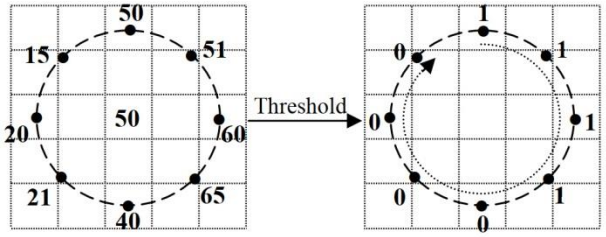

Fig. 4. Local binary pattern operator.

The LBP operator takes the form:

$$LBP(x_c,y_c)= \sum_{n=0}^{7} 2^n S(i_n-i_c) \quad (1)$$

where in this case n runs over the eight neighbors of the central pixel c, i_c and in are the gray-level values at c and n. Function S(x) is s defined below,

$$S(x) = \begin{cases} 1 & if \ x \geq 0 \\ 0 & if \ x < 0 \end{cases} \quad (2)$$

The LBP operator uses a method that employs only the use of the sign of the difference between two gray values, which sometimes leads to a failure to generate binary codes consistent with the texture properties for the local region (Fig. 5). To avoid this handicap, a variant of this operator will be used. This variant assigns a 2P binary code to the central pixel according to the gray values of the local neighborhood comprising P neighbors; this method is Compound Local Binary Pattern (CLBP) [47]. The CLBP operator uses two bits for each neighbor to encode the sign as well as the magnitude information of the difference between the center and the neighboring gray values, unlike the LBP which uses only one bit for each neighbor by representing the sign of the difference between the center and the corresponding neighboring gray values. In this method, the first bit represents the sign of the difference between the center and the corresponding neighboring gray values as the basic LBP encoding. The second bit is used to encode the magnitude of the difference with respect to a threshold value, which is the average magnitude M_{avg} of the difference between the central and neighboring gray values in the local neighborhood of interest. The CLBP operator chooses the value 1 for the second bit if the magnitude of the difference between the center and the corresponding neighbor is greater than the threshold M_{avg}. Otherwise, it takes the value 0. Thus, the s(x) indicator of equation 2 is replaced by the function below:

$$s(i_p, i_c) = \begin{cases} 00 \ ip-ic<0, & |i_p-i_c| \leq M_{avg} \\ 01 \ ip-ic<0 & |i_p-i_c| > M_{avg} \\ 10 \ ip-ic \geq 0, & |i_p-i_c| \leq M_{avg} \\ 11 & otherwise \end{cases} \quad (3)$$

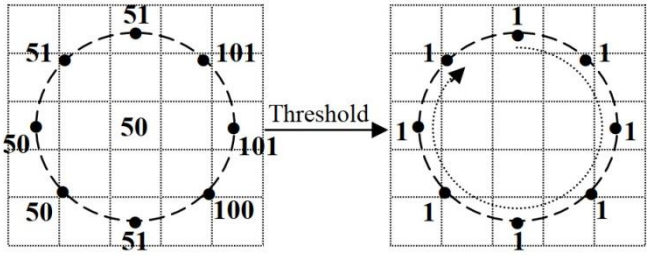

Fig. 5. Generation of inconsistent binary pattern in LPB.

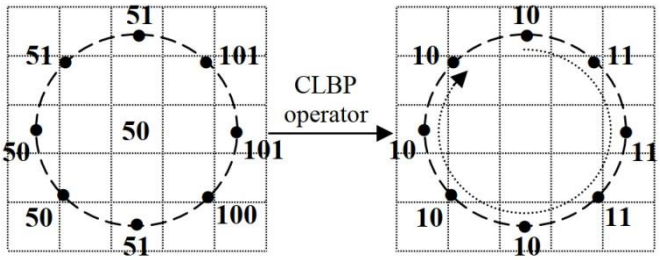

Fig. 6. Compound local binary pattern operator.

where i_c and i_p are the gray values of the central pixel and the neighbors, and the average magnitude of the difference between i_p and i_c in the local neighborhood is M_{avg}. The mechanism of the CLBP operator is shown in the Fig. 6.

B. Matching Process Phase

The choice of classifiers is crucial for a better performance concerning the proposed approach, to ensure this important phase in all recognition systems, we relied on two important factors. The first factor depends on the resolution of the images used, which is low, classifiers like SVM will be disregard, because are more for high resolutions [51, 52]. The second factor is also important, it depends on the computation time costs, which represents a decisive point for the success of a recognition mechanism; these points will direct our choice towards distance-based classifiers. The consideration of the directives already mentioned, directed the choice towards a set including three classifiers based on the distance, which we will use with the method of extraction employed and see their performances for the generation of the recognition rates. These classifiers are based on Euclidean distance, City-block and Jeffrey Divergence.

The Euclidean distance is the best-known distance metric and used in datasets that represent low-dimensional images, examines the root of the squared differences between the coordinates of a pair of objects. This process is generally known as the Pythagorean Theorem. For the tests, we used this classifier, to calculate the minimum distance between the test image and the train image. The Euclidean distance d is as follows:

$$d(x,y) = \sqrt{\sum_{i=1}^{n}(x_i - y_i)^2} \quad (4)$$

The Manhattan distance classifier, city-block distance classifier, also called, rectilinear distance, L1 distance, L1 norm, Manhattan length. It represents the distance between points in a city road grid. It examines the absolute differences between the coordinates of a pair of objects as follows:

$$d(x,y) = \sum_{i=1}^{n}| x_i - y_i| \quad (5)$$

The Jeffrey divergence is a modification of the Kullback-Leibler (KL) divergence, if P = (p_1, . . . p_N) and Q = (q_1, . . . q_N) are two discrete distributions, the Jeffrey divergence between P and Q is defined as:

$$D(P,Q) = \sum_i (p_i \ log \frac{P_i}{m_i} + q_i \ log \frac{q_i}{m_i} \quad (6)$$

$$\text{Where} \quad m_i = \frac{(p_i + q_i)}{2}$$

III. Experimental Result

In this part, an experimental study spread over several stages will be made. The objective of these steps will be articulated on the progressive demonstration of the process reliability for the proposed system. The evaluation of this system will be conducted on the Casia multispectral palmprint database [46]. It should be noted that this database is one of the standards of scientific research in this field.

A. Casia Multispectral Palmprint Database

The construction of the CASIA Multi-Spectral Palmprint database is based on the acquisition of 7200 palmprint images from 100 volunteers. This set of images is shared equally between the palms of the right hand and the left hand (3600 images on each hand). It should be noted that the set of palmar images for each hand is captured in two sessions. The time between the two capture sessions has an interval greater than one month. During a session, each volunteer gives three samples for each hand (a total of six images per user in a single session, so 600 images for 100 volunteers). Each image of a sample is captured with six different electromagnetic spectrums (Fig. 7). The wavelengths used for these captures correspond to the following six spectrums: white light (WL), 460 nm, 630 nm, 700 nm, 850 nm and 940 nm. The captures have been made in such a way that the user has a certain freedom for the pose concerning the angle and the rotation of his hand, the goal is to produce variations of hand postures during the capture session. This procedure will simulate a use that is done in the real world and increase the diversity of samples in the same class, which will present interesting challenges for measuring the performance of a biometric system. It is reminded that the palm images captured are 8-bit grayscale JPEG files.

Generally, the biometric database preparation follows a process that relies on two phases; the first concerns the acquisition of images over different time intervals and the second revolves around preprocessing mechanisms, that can vary depending on the modality nature and the objectives targeted by the research conducted.

A careful examination of the database images reveals two important factors that will direct our preprocessing towards an extraction of the regions of interest; the first is seen on the capture of hands that will undergo changes (Hand with Corn, Callosity, Induration) due to manual work or intense physical activities in strength sports such as bodybuilding or powerlifting (Fig. 8).

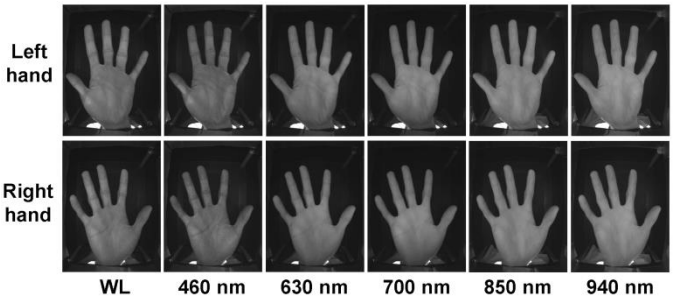

Fig. 7. Casia multipectral palmprint database.

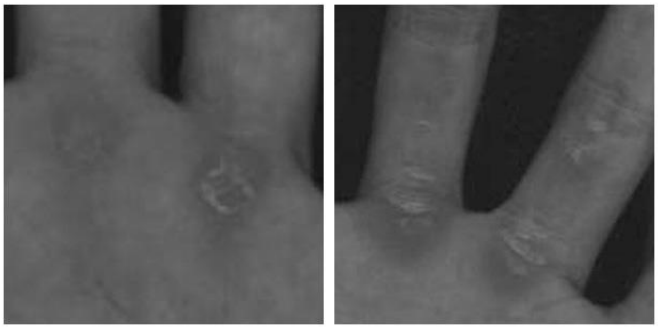

Fig. 8. Images with corn, callosity and induration in casia multipectral palmprint database.

The second factor is noticeable in the images where the pose of the hand for capture is free and not standardized. This hand posing manner (flexion hand) may in some cases present angles with respect to the capture support, which cause the relevant features at the level of the hand palm contour to be inhibited, the same in the case of the poses of the hand which have a concavity (Fig. 9).

Fig. 9. Poses with flexion and concavity in casia multipectral palmprint database.

These two factors may skew experimental results, on the one hand, the change that certain parts of hand palm may undergo, which increases intra-class variations, on the other hand, the absence of relevant features on areas of the hand palm, which may increase the interclass similarities of the histograms with the local methods. To avoid these problems, it

is essential to carry out a pre-processing which aims at extracting the regions of interest ROI. This process of regions of interest extraction will be used to solve the problems of the Casia Multi-spectral Palmprint database images already mentioned. Indeed, the principle aims to adjust the rotation of different angles and the normalization of the scales, then to carry out a cropping on the normalized image central region to extract the relevant characteristics. It is obvious that an ROI extraction method that is based on a good algorithm will be decisive in generating palm prints images with zones, which allow the maximum of distinctive characteristics. This effect will have a significant impact on the performance of the recognition system to be built. The majority of existing methods use algorithms that perform an ROI extraction based on the limit of the palm, or key landmarks between the fingers, or some external factors [53, 54].

Many existing palmprint recognition mechanisms assume that palmprint images are aligned before performing feature extraction and matching. Because of this, they are often affected by residual variations in translation and rotation after the alignment process. To avoid this problem, the Principal Based ICP [48] will be employed, this method uses the linear features to refine the alignment of the image before performing the cropping operation to extract Region of Interest (ROI) images (Fig. 10).

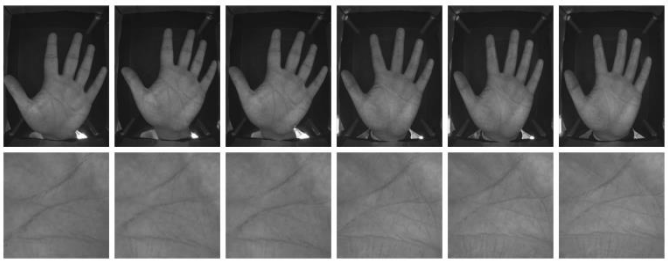

Fig. 10. Casia multipectral palmprint ROI database.

B. Evaluation and Analysis of Experimental Results

To approve the recognition mechanism, we opted for an evaluation process divided into three different parts. The first part focuses on the extraction of ROI images with the Principal Based ICP method for a crop of 192x192 pixels and verifying the ability of the chosen classifiers to offer efficient results with the extraction method adopted. In this phase, several detailed experiments for each hand (left and right) will be carried out and which will have as a goal; the determination of the classifiers most adapted to this kind multi-spectral images, this adaptation will obviously be evaluated on two points: the first concerns the recognition rates obtained and the second point concerns the duration of the calculations necessary for the matching process concerning all the classes. In the second part, the resolution adopted for the ROI images will be changed. The resolution will become 128x128 pixels instead of 192x192 pixels. After obtaining the results of this new phase, we will compare them with the previous phase and we will proceed to the analysis of the data to draw conclusions concerning the impact of the resolution of the global image. In the case where the impact of this operation represents positive points in terms of performance and computation time, it will be adopted for the rest of the experiments. Finally, in the last part, the conclusions obtained in the global approach will be used, the final experimental results of the proposed approach will be examined and the conclusions on the obtained reliability will be drawn.

1) Multispectral palmprint evaluation: During this first step, the system will be evaluated. It should be noted that the Casia database presents images in the same class, which represent concavities during the pose and varying angles depending on the capture pose, these factors increase the intra-class variation. For this, an experimental protocol which will respect the real conditions will be used (Fig. 11). The training database will be composed of five images per user and the test database will be composed of a single image per user (as in the real case to ensure the operation in the devices implemented). Therefore, for each volunteer, there are five training samples and one test sample for each spectrum. The proposed approach is based on local techniques. Therefore, the performance of the mechanism will be examined with different sizes of sub-images.

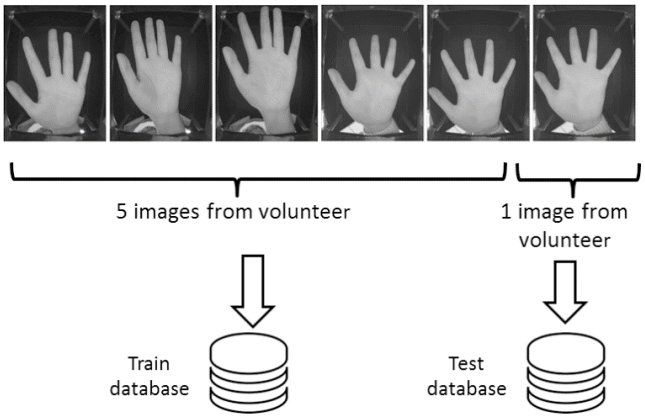

Fig. 11. Protocol used for experiments.

Block subdivision sizes have been classified into three categories: large subdivision, medium subdivision, and small subdivision. The large subdivision is defined by two block sizes: 64x64 and 48x48 pixels, for the medium size: 32x32 and 24x24 pixels, and for the small size: 16x16 and 8x8 pixels. To ensure a better performance of the classification process of the proposed approach, several classifiers based on Euclidean distance, Jeffrey divergence and City-Block was experimented. The recognition rates for each palmprint with the image sub-divisions chosen for the different spectra will be presented later in tables. This comparative evaluation is made in order to show the most adaptive classifiers in our case and the cost in computation time.

a) Result of experiment with cropping 192x192 resolution: In this first phase of the experiments, we will use the diagram Fig. 1 with the resolution 192x192 pixels for the images obtained from the cropping made by Principal Based ICP method. This phase aims to evaluate the extraction method, the classifiers used and their impact on Matching Process Time (MPT) with all the spectrums: white light, 460nm, 630nm, 700nm, 850nm and 940nm.

TABLE I. RECOGNITION RATE FOR LEFT PALM - WHITE LIGHT

Table Recognition rate RR for left palm with white light				
Block size	***RR/MPT***	***Euclidian distance***	***Jeffrey divergence***	***City-Block***
64x64	RR	74%	**82%**	81%
	MPT	0,079923 s	4,801806 s	0,139913 s
48x48	RR	79%	**85%**	83%
	MPT	0,085569 s	8,424969 s	0,215667 s
32x32	RR	83%	**87%**	**87%**
	MPT	0,143411 s	18,388208 s	0,431222 s
24x24	RR	85%	**89%**	**89%**
	MPT	0,224072 s	31,534391 s	0,734840 s
16x16	RR	87%	**92%**	**92%**
	MPT	0,414146 s	64,496038 s	1,608370 s
8x8	RR	78%	**92%**	89%
	MPT	1,774764 s	166,262356 s	6,320234 s

This Table I, clearly shows that the recognition rates (RR) obtained by the classifiers based on the city-block distance and the Jeffery divergence are clearly better than those obtained by the classifier based on the Euclidean distance. The classifiers based on the city-block distance and the Jeffery divergence give the best value of recognition rate 92% for the divisions (sub-images) of 8x8 and 16x16 pixels. We also note that the Matching Process Time MPT increases proportionally to the decrease in the size of the division block. This remark is logical, since the smaller the block size, the more the number of sub-images increases, and consequently the histogram of the image too. It should be noted that despite the similar performance shown by the classifier based on Jeffrey divergence (92%) with the 16x16 pixel block compared to that obtained with city-block (92%), nevertheless, the overall computation time for the set of classes is high (64.496038 s) compared to the city-block distance based classifier (1.608370 s).

We can conclude that even if the rates obtained with Jeffrey diverge and city-block are almost similar, the ratio (recognition rate \ calculation time) remains in favor of city-block. In the following, we are going to join on the same table the recognition rates of the left and right palm prints (resolution 192x192) and no longer record the calculation time, since we already know the behavior of the calculation time with the Table I.

For the right palm (R Palm), Table II shows the same remarks as the left palm (L Palm), the superiority of the classifiers based on the Jeffrey divergence and the City-block, and that the computation time is privileged for the city-block. Note that the value of the high recognition rate is **97%** with Jeffrey divergence for block size 8x8 pixels.

In Table III, the results obtained affirm that the resulting recognition rates with the classifiers based on the Jeffrey divergence and the City-block are the best. Note that the value of the high recognition rate obtained is 91% with city block for a block of size 8x8 pixels with Left palm and 98% with right palm.

In Table IV, we have the same previous remarks, the superiority of the classifiers based on Jeffrey divergence and the City-block is maintained. Note that the value of the high recognition rate obtained is 88% with Jeffrey divergence for a block of size 24x24 pixels with left palm and 100% with Jeffrey divergence for a block of size 8x8 pixels with right palm. City-block also shows similar results: 99% for a block of size 8x8, 16x16 and 24x24 pixels with right palm, and 87% for a block of size 16x16 and 24x24 pixels with left palm.

TABLE II. RECOGNITION RATE - WHITE LIGHT

Table Recognition rate RR for left and right palm with white light						
Block size	***Euclidian distance***		***Jeffrey divergence***		***City-Block***	
	L Palm	***R Palm***	***L Palm***	***R Palm***	***L Palm***	***R Palm***
64x64	74%	63%	82%	80%	81%	81%
48x48	79%	76%	85%	89%	83%	87%
32x32	83%	80%	87%	92%	87%	91%
24x24	85%	87%	89%	95%	89%	94%
16x16	87%	90%	**92%**	96%	**92%**	95%
8x8	78%	87%	**92%**	**97%**	89%	96%

TABLE III. RECOGNITION RATE – SPECTRUM 460

Table Recognition rate RR for left and right palm - spectrum 460nm						
Block size	***Euclidian distance***		***Jeffrey divergence***		***City-Block***	
	L Palm	***R Palm***	***L Palm***	***R Palm***	***L Palm***	***R Palm***
64x64	77%	76%	87%	87%	85%	84%
48x48	81%	81%	88%	92%	87%	90%
32x32	84%	85%	90%	96%	89%	94%
24x24	85%	95%	88%	96%	88%	96%
16x16	87%	96%	89%	97%	89%	97%
8x8	86%	90%	90%	96%	**91%**	**98%**

TABLE IV. RECOGNITION RATE – SPECTRUM 630

Table Recognition rate RR for left and right palm - spectrum 630nm						
Block size	***Euclidian distance***		***Jeffrey divergence***		***City-Block***	
	L Palm	***R Palm***	***L Palm***	***R Palm***	***L Palm***	***R Palm***
64x64	72%	76%	84%	89%	80%	87%
48x48	74%	83%	85%	95%	83%	92%
32x32	84%	90%	86%	97%	87%	97%
24x24	85%	93%	**88%**	98%	87%	99%
16x16	79%	95%	87%	99%	87%	99%
8x8	69%	87%	86%	**100%**	83%	99%

TABLE V. RECOGNITION RATE – SPECTRUM 700

Table Recognition rate RR for left and right palm - spectrum 700nm						
Block size	*Euclidian distance*		*Jeffrey divergence*		*City-Block*	
	L Palm	*R Palm*	*L Palm*	*R Palm*	*L Palm*	*R Palm*
64x64	72%	77%	86%	85%	83%	82%
48x48	80%	81%	86%	91%	85%	86%
32x32	80%	88%	87%	96%	85%	95%
24x24	85%	88%	90%	95%	89%	95%
16x16	80%	88%	**91%**	95%	90%	94%
8x8	73%	81%	88%	**97%**	87%	93%

In Table V, we note again the superiority of the classifiers based on the Jeffrey divergence and the City-block. Note that the value of the high recognition rate obtained is 91% with Jeffrey divergence for a block of size 16×16 pixels with left palm, and 97% for a block of size 8x8 pixels with right palm.

TABLE VI. RECOGNITION RATE – SPECTRUM 850

Table Recognition rate RR for left and right palm - spectrum 850nm						
Block size	*Euclidian distance*		*Jeffrey divergence*		*City-Block*	
	L Palm	*R Palm*	*L Palm*	*R Palm*	*L Palm*	*R Palm*
64x64	73%	75%	92%	94%	87%	92%
48x48	84%	88%	94%	96%	92%	96%
32x32	86%	92%	93%	96%	93%	97%
24x24	89%	94%	94%	**98%**	**95%**	**98%**
16x16	86%	98%	94%	**98%**	94%	**98%**
8x8	68%	81%	**95%**	**98%**	91%	**98%**

In Table VI, the superiority of classifiers based on Jeffrey divergence and City-block is maintained. Note that the value of the high recognition rate is 95% with Jeffrey divergence for a block of size 8x8 pixels and City-block for a block of size 24x24 pixels, the same for the right palm; we notice that the highest recognition rate is obtained with Jeffrey divergence and City-block for the blocks: 8x8, 16x16 and 24x24 pixels.

TABLE VII. RECOGNITION RATE – SPECTRUM 940

Table Recognition rate RR for left and right palm - spectrum 940nm						
Block size	*Euclidian distance*		*Jeffrey divergence*		*City-Block*	
	L Palm	*R Palm*	*L Palm*	*R Palm*	*L Palm*	*R Palm*
64x64	77%	74%	89%	92%	85%	88%
48x48	85%	83%	93%	95%	89%	93%
32x32	86%	92%	**94%**	97%	92%	97%
24x24	91%	94%	93%	**98%**	**94%**	97%
16x16	90%	97%	**94%**	**98%**	**94%**	**98%**
8x8	80%	89%	93%	**98%**	**94%**	**98%**

Finally, for the 940nm spectrum, Table VII again shows the superiority of the classifiers based on the Jeffrey divergence and the City-block. Note that the value of the higher recognition rate is 94% with Jeffrey and City-block divergence for different block sizes: 8x8, 16x16, 24x24 and 32x32 pixels with left palm. We notice the same thing for the right palm, note that the value of the higher recognition rate is 98% with Jeffrey and City-block divergence for different block sizes: 8x8, 16x16pixels.

In summary, we can draw up the following two tables which summarize the recognition rates obtained for all spectrums.

TABLE VIII. BETTER RECOGNITION RATES FOR LEFT PALM – 192X192 RESOLUTION

Table Recognition rate RR for left palm						
Block size	**8x8**	**16x16**	**24x24**	**32x32**	**48x48**	**64x64**
White light	**92%**	**92%**	89%	87%	85%	82%
460 nm	91%	89%	88%	90%	88%	87%
630 nm	86%	87%	88%	86%	85%	84%
700 nm	88%	91%	90%	87%	86%	86%
850 nm	**95%**	94%	**95%**	93%	94%	92%
940 nm	**94%**	**94%**	94%	94%	93%	89%

TABLE IX. BETTER RECOGNITION RATES FOR RIGHT PALM – 192X192 RESOLUTION

Table Recognition rate RR for left palm						
Block size	**8x8**	**16x16**	**24x24**	**32x32**	**48x48**	**64x64**
White light	**97%**	**96%**	**95%**	92%	89%	81%
460 nm	**98%**	**97%**	**96%**	**96%**	92%	87%
630 nm	**100%**	**99%**	**99%**	**97%**	95%	89%
700 nm	**97%**	**95%**	**95%**	**96%**	91%	85%
850 nm	**98%**	**98%**	**98%**	**97%**	**96%**	94%
940 nm	**98%**	**98%**	**98%**	**97%**	**95%**	92%

Both Tables VIII and IX show promising recognition rates for the proposed mechanism which vary between 81% and 100%. We also see the superiority of the results obtained with palm prints of the right hand. We can also say that on average the spectrums that give the best results for both hands are the 850nm and 940nm spectra with the exception of the 630nm spectrum for the right hand. It should also be noted that the (recognition rate / global computation time) ratio remains in favor of City-block.

b) Result of experiment with resizing 128x182 resolution: Based on the previous conclusions concerning the computation time, and the pattern characteristics of the regions of interest of the palmprints which show clearly visible and large-scale features, we thought that there is a relationship between cropping resolution and the performance of the proposed approach which is based on local methods. This assumption comes from the fact that if we have a high resolution with little relevant information, then we will have division blocks that will be similar between the different classes and therefore a reduction in recognition rates. This is what we will try to dismantle with the following experiments.

In the following we will resize images from 192x192 pixels to 128x128 pixels. The results of previous experiments will guide future experiments towards small and medium-sized blocks, which give reliable recognition rates. The second orientation concerns the choice of 940nm, this choice is due to the fact that the 940nm spectrum shows the veins of the palm which makes the system robust to the temptations of fraud and it has shown good results. The last orientation concerns the 460 nm spectrum, this spectrum best show the characteristics of the pattern and it shows a good performance against white light. The results of these choices will help in the construction of the final mechanism.

At the beginning, we will experiment with white light for left palm, to study the improvement brought with this resize.

TABLE X. RECOGNITION RATE FOR LEFT PALM – WHITE LIGHT

Table Recognition rate RR for left palm – white light				
Block size	*RR/MPT*	*Euclidian distance*	*Jeffrey divergence*	*City-Block*
32x32	RR	82%	**88%**	86%
	MPT	0,067901 s	5,478638 s	0,142141 s
24x24	RR	85%	**92%**	91%
	MPT	0,095663 s	10,647785 s	0,257458 s
16x16	RR	88%	**93%**	91%
	MPT	0,160716 s	19,651213 s	0,472513 s
8x8	RR	86%	91%	**93%**
	MPT	0,524071 s	53,258396 s	1,867898 s

The Table X shows a clear reduction in the calculation time compared to the 192x192 resolution, we cite as an example 166.262356 s (8x8 Jeffrey divergence in 192x192) and 6.320234s (8x8 City-block in 192x192) which will be reduced to 53,258396 s (8x8 Jeffrey divergence in 128x128) and 1,867898s (8x8 City-block in 128x128). Similarly the recognition rates have been improved. Note that the value of the high recognition rate is 93% with Jeffrey divergence for block size 16x16 pixels and City-block for block size 8x8 pixels against 92% obtained with Jeffrey divergence for block size 8x8 with 192x192 (cropping resolution) and MPT= 166.262356 s. In the rest of the experiments, we will no longer put the calculation times in the tables; we know very well that it will be significantly reduced.

TABLE XI. RECOGNITION RATES FOR 128X128– WHITE LIGHT

Table Recognition rate RR for left and right palm – white light						
Block size	*Euclidian distance*		*Jeffrey divergence*		*City-Block*	
	L Palm	*R Palm*	*L Palm*	*R Palm*	*L Palm*	*R Palm*
32x32	82%	80%	88%	95%	86%	94%
24x24	85%	87%	92%	97%	91%	95%
16x16	88%	98%	**93%**	98%	91%	98%
8x8	86%	95%	91%	98%	**93%**	**99%**

We note in Table XI, the superiority of the Jeffrey divergence and the City-block classifiers, and the value of the highest recognition rate is 99% City-block for blocks of size 8x8 with right palm and 93% with left palm.

TABLE XII. RECOGNITION RATES FOR 128X128– SPECTRUM 460

Table Recognition rate RR for left and right palm - spectrum 460nm						
Block size	*Euclidian distance*		*Jeffrey divergence*		*City-Block*	
	L Palm	*R Palm*	*L Palm*	*R Palm*	*L Palm*	*R Palm*
32x32	85%	93%	92%	99%	92%	99%
24x24	87%	96%	**95%**	99%	**95%**	99%
16x16	92%	**100%**	93%	99%	93%	99%
8x8	89%	89%	93%	**100%**	**95%**	**100%**

The Table XII shows good value rates, the value of the high recognition rate is 95% with Jeffrey divergence and City-block for blocks of size 8x8 pixels and 24x24, similarly, for the right palm we have perfect value rates, the value of the high recognition rate is 100% with Jeffrey divergence and City-block for blocks of size 8x8 pixels.

TABLE XIII. RECOGNITION RATES FOR 128X128– SPECTRUM 940

Table Recognition rate RR for left and right palm - spectrum 940nm						
Block size	*Euclidian distance*		*Jeffrey divergence*		*City-Block*	
	L Palm	*R Palm*	*L Palm*	*R Palm*	*L Palm*	*R Palm*
32x32	76%	85%	95%	97%	92%	94%
24x24	86%	91%	94%	**98%**	95%	96%
16x16	89%	93%	94%	**98%**	**96%**	**98%**
8x8	81%	92%	93%	**98%**	94%	**98%**

Table XIII also shows good value rates, the high recognition rate value is 96% City-block for blocks of size 16x16 with the left palm. With regard to the right palm, we have effective value rates; the value of the high recognition rate is 98% with Jeffrey and City-block divergence for blocks of size 8x8 pixels, 16x16 and 24x24 pixels.

The results of the experiments confirmed that resizing the resolution of the crop to 128x128 instead of 192x192 pixels improved the performance of the recognition rates and reduced the calculation time. This is normal, since image databases will have small sizes, this resizing will have a significant impact in the real world for large populations. The blocks that show the best performance are 8x8, 16x16 and 24x24 pixels, which is normal since we are using a local method for feature extraction. Large size subdivisions are not efficient for this kind of methods, henceforth we will only use the 8x8, 16x16 and 24x24 pixel blocks for the remaining experiments.

C. Global Evaluation of Proposed Approach

In this section, we will conduct our experiments to evaluate the proposed approach (Fig. 3). These experiments consist in exploiting the sizes of the blocks, which have shown their performance previously (24x24, 16x16 and 8x8). In this evaluation, we will use the approach with a score-level fusion, with city-block distance and Jeffrey divergence. We will use the Cumulative Matching Characteristics (CMC) curves for

each fusion case to measure the identification accuracy. CMC curves demonstrate the ability of a recognition system to identify a given user in a set of data.

1) Results of fusion left palmprint 460nm and left palmprint 940

a) Results for block size 8x8 pixels: In Fig. 12, we notice that the curves resulting from the fusion of the 460nm + 940nm multi-spectral images with the classifiers with Jeffrey divergence and city-block are clearly higher than the other curves. The recognition rate obtained with the approach equal to 100%, this rate is higher than the best rate obtained for the systems studied with a single spectrum.

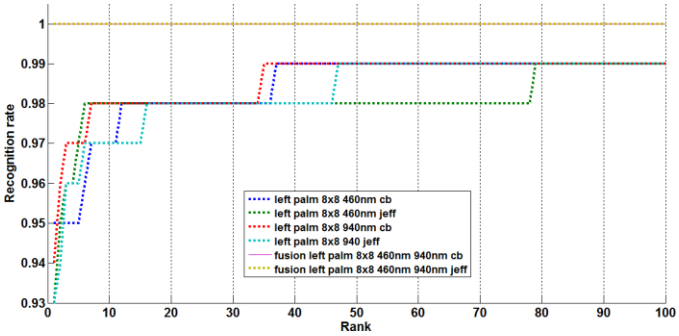

Fig. 12. CMC curve for fusion 460nm+940nm with 8x8 blocks.

b) Results for block size 16x16 pixels: In Fig. 13, we will report the same remark in the case of the block equal to 8x8. The recognition rate obtained with the approach is equal to 99%, this rate is higher than the best rate obtained for the systems studied previously.

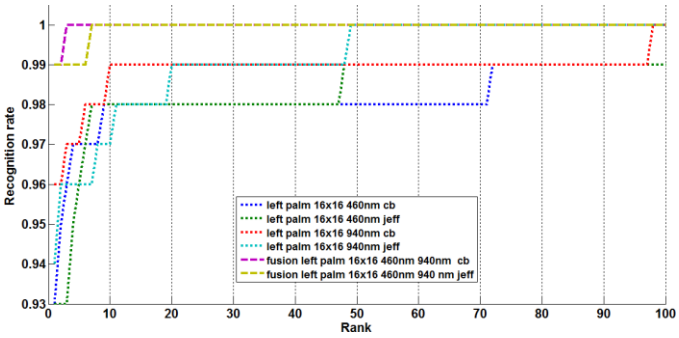

Fig. 13. CMC curve for fusion 460nm+940nm with 16x16 blocks.

c) Results for block size 24x24 pixels: In Fig. 14, we notice that the curve resulting from the fusion of the 460nm + 940nm multi-spectral images with the classifier based on city-block is superior to the other curves, but this is not the case of the fusion curve which uses the classifier based on Jeffrey's divergence. The recognition rate obtained with the approach equal to 100% using the classifier based on the city-block distance, this rate is higher than the best rate obtained for the systems studied with a single spectrum.

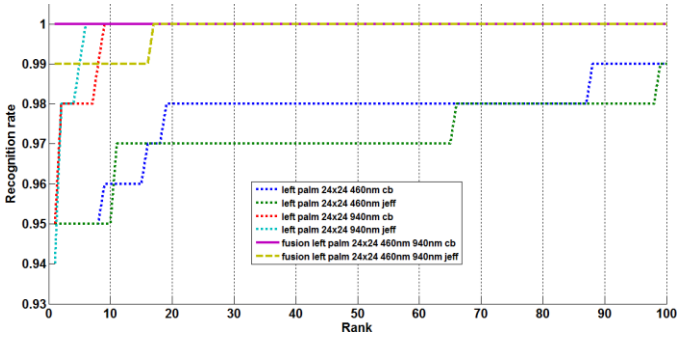

Fig. 14. CMC curve for fusion 460nm+940nm with 24x24 blocks.

TABLE XIV. RESULTS OF GLOBAL APPROACH FOR LEFT PALM

Recognition rate for left palm – fusion with spectrums 460 and 940		
Block size	***Jeffrey divergence***	***City-Block***
24x24	99%	**100%**
16x16	**99%**	**99%**
8x8	100%	**100%**

The Table XIV summarizes the performance obtained by the global approach used.

2) Results of fusion right palmprint 460nm and right palmprint 940

a) Results for block size 8x8 pixels: In the Fig. 15, we have perfect recognition rates for fusion equal to 100%.

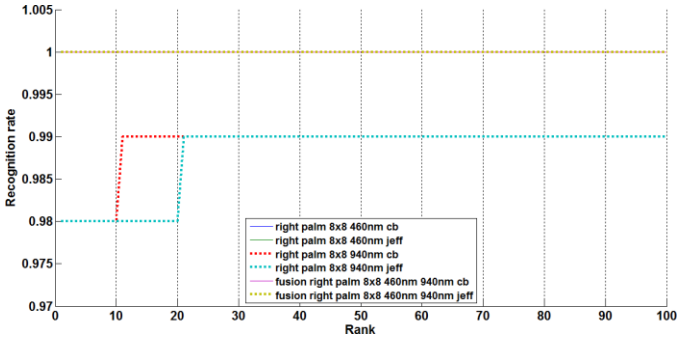

Fig. 15. CMC curve for fusion 460nm+940nm with 8x8 blocks.

b) Results for block size 16x16 pixels: In Fig. 16, we still have perfect recognition rates for fusion equal to 100%, which demonstrates the robustness and efficiency of the proposed approach.

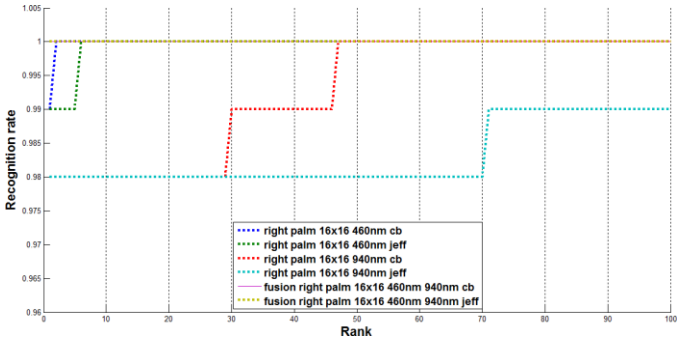

Fig. 16. CMC curve for fusion 460nm+940nm with 16x16 blocks.

c) Results for block size 24x24 pixels: In Fig. 17, we still notice that the curves resulting from the fusion of the 460nm + 940nm multi-spectral images with the classifiers with Jeffrey divergence and city-block are clearly higher than the other curves. The recognition rate obtained with the approach equal to 99%, this rate is higher than the best rate obtained for the systems studied with a single spectrum.

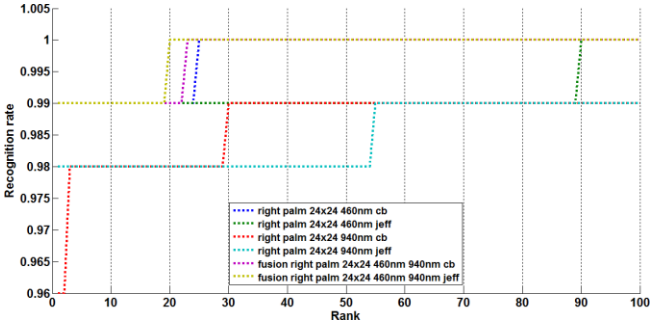

Fig. 17. CMC curve for fusion 460nm+940nm with 24x24 blocks.

TABLE XV. RESULTS OF GLOBAL APPROACH FOR RIGHT PALM

Recognition rate for right palm – fusion with spectrums 460 and 940		
Block size	***Jeffrey divergence***	***City-Block***
24x24	99%	**99%**
16x16	**100%**	**100%**
8x8	**100%**	**100%**

The Table XV summarizes the performance obtained by the global approach used for right palm.

The results demonstrated by the experiments that we see in the CMC curves, on the Tables XIV and XV and the comparison with others methods in Table XVI, reflect the effectiveness of the approach used to build a reliable and robust recognition system.

TABLE XVI. A COMPARISON OF RECOGNITION RATE OF THE PROPOSED APPROACH AND PREVIOUS METHODS

Method	**Recognition rate**
EigenPalm (EP) [55]	91,25%
FisherPalm (FP) 55]	92,32%
Gabor-based RCM (GRCM) [55]	96%
Enhanced GRCM (EGRCM) [55]	98%
Image level fusion by PCA [56]	95,17%
Quaternion PCA [56]	98,13%
Quaternion PCA+Quaternion DWT [56]	98,83%
PCA on HOG [57]	98,73%
KPCA on HOG [57]	98,737%
Proposed approach (using 24x24 bloc)	**99%**
LDA on HOG [57]	99,17%
KLDA on HOG [57]	99,17%
PCA on HOL [57]	99,73%
KPCA on HOL [57]	99,73%
Proposed approach (using 16x16 and 8x8 blocs)	**100%**

IV. CONCLUSION

In this work, multi-spectral images are used with different spectrums to build a secure system against tampering maneuvers. In this sense, two instances are employed with two spectrums that can be captured at the same time (but sequentially), to be used in a score-based fusion approach. The experimental results were conducted on the casia multispectral database after pre-processing with the Principal Based ICP method, subsequently the cropping used was improved for an optimal construction of the histograms, which made it possible to increase the performance and to reduce the calculation time, Finally, the conclusions drawn were deployed to guide the proposed approach, which clearly showed its effectiveness with rates varying between 99% and 100%. Thus, it is possible to conclude that this approach provides proven reliability and can be used for secure fingerprint recognition systems against fingerprint forgery fraud. This work aims at the possibilities of securing during the "capture" phase, nevertheless this securing will have to affect other aspects such as the base of the images. This perspective will be the subject of future work on securing biometric images with watermarking methods.

REFERENCES

[1] Buciu, I.; Gacsadi, A. Biometrics systems and technologies: A survey. Int. J. Comput. Commun. Control 2016, 11, 315–330.

[2] E. J. Kindt, “An introduction into the use of biometric technology,” in Privacy and Data Protection Issues of Biometric Applications: A Comparative Legal Analysis. Springer Netherlands, 2013, pp. 15-85.

[3] Thejaswini P, Srikantaswamy R S and Manjunatha A S, “Novel Adaptive Auto-Correction Technique for Enhanced Fingerprint Recognition” International Journal of Advanced Computer Science and Applications (IJACSA), 10(8), 2019.

[4] Mostofa, M.; Mohamadi, S.; Dawson, J.; Nasrabadi, N.M. Deep GAN-based cross-spectral cross-resolution iris recognition. IEEE Trans. Biomet. Behav. Identity Sci. 2021, 3, 443–463.

[5] A. Amraoui, M. Ait Kerroum and Y. Fakhri, “Multi-instance Finger Knuckle Print Recognition based on Fusion of Local Features” International Journal of Advanced Computer Science and Applications(IJACSA), 13(9), 2022.

[6] D. Prabakaran and R. Shyamala, “A Review On Performance Of Voice Feature Extraction Techniques,” 2019 3rd International Conference on Computing and Communications Technologies (ICCCT), 2019, pp. 221-231.

[7] Mahalakshmi B S and Sheela S V, “A Novel Feature Extraction for Complementing Authentication in Hand-based Biometric” International Journal of Advanced Computer Science and Applications (IJACSA), 12(9), 2021.

[8] R.M. Bolle, J.H. Connell, S. Pankanti, N.K. Ratha, A.W. Senior, Guide to Biometrics: Selection and System Design, Springer, Boston, MA, 2003.

[9] Ammour, B.; Boubchir, L.; Bouden, T.; Ramdani, M. Face–iris multimodal biometric identification system. Electronics 2020, 9, 85.

[10] J. Priesnitz, R. Huesmann, C. Rathgeb, N. Buchmann, C. Busch “Mobile contactless fingerprint recognition: implementation, performance and usability aspects” Sensors, 22 (3) (2022), pp. 1-21.

[11] Y. Xu, G. Lu, Y. Lu, and D. Zhang, "High resolution fingerprint recognition using pore and edge descriptors," Pattern Recognition Letters, vol. 125, pp. 773-779, Jul. 2019.

[12] S. A. Shawkat, K. S. L. Al-badri, and A. I. Turki, "The new hand geometry system and automatic identification," Periodicals of Engineering and Natural Sciences, vol. 7, no. 3, pp. 996-1008, 2019.

[13] Angadi, S. and S. Hatture, Hand geometry based user identification using minimal edge connected hand image graph. IET Computer Vision, 2018. 12(5): p. 744-752.

[14] Muthukumar, A., Kavipriya, A, "A biometric system based on Gabor feature extraction with SVM classifier for Finger-Knuckle-print", Pattern Recognition Letters, 2019, 125, pp. 150– 156.

[15] Kim, J.; Oh, K.; Oh, B.S.; Lin, Z.; Toh, K.A. A line feature extraction method for finger-knuckle-print verification. Cognitive Computation 2019, 11, 50–70.

[16] Matkowski W.M., Chai T., Kong A.W.K., Palmprint recognition in uncontrolled and uncooperative environment, IEEE Transactions on Information Forensics and Security. 15 (2019) 1601–1615.

[17] S. Zhao and B. Zhang, "Deep discriminative representation for generic palmprint recognition," Pattern Recognition, vol. 98, p. 107071, 2020.

[18] A. Amraoui, Y. Fakhri and M. A. Kerroum, "Unimodal palmprint recognition system based on local features," 2017 International Conference on Advanced Technologies for Signal and Image Processing (ATSIP), 2017, pp. 1-5.

[19] T. Chugh, K. Cao, and A. K. Jain, "Fingerprint spoof buster: Use of minutiae-centered patches," IEEE Trans. Information Forensics and Security, 2018.

[20] Chen, H.; Chen, Y.; Tian, X.; Jiang, R. "A Cascade Face Spoofing Detector Based on Face Anti-Spoofing R-CNN and Improved Retinex LBP". IEEE Access 2019, 7, 170116–170133.

[21] D. Zhang, Z. Guo, G. Lu, L. Zhang, and W. Zuo, "An online system of multispectral palmprint verification," IEEE Transactions on Instrumentation and Measurement, vol. 59, no. 2, pp. 480–490, 2010.

[22] W. Jia, B. Zhang, J. Lu, Y. Zhu, Y. Zhao, W. Zuo, H. Ling, "Palmprint Recognition Based on Complete Direction Representation," IEEE Transaction on Image Processing, vol. 26, no. 9, pp. 4483–4498, 2017.

[23] A. Kong, D. Zhang, and M. Kamel, "Palmprint identification using feature-level fusion," Pattern Recognition, vol. 39, no. 3, pp. 478–487, 2006.

[24] W. Jia, D.-S. Huang, and D. Zhang, "Palmprint verification based on robust line orientation code," Pattern Recognition, vol. 41, no. 5, pp. 1521–1530, 2008.

[25] D. Hong, W. Liu, J. Su, Z. Pan, and G. Wang, "A novel hierarchical approach for multispectral palmprint recognition," Neurocomputing, vol. 151, no. 1, pp. 511–521, 2015.

[26] L. Fei, Y. Xu, and D. Zhang, "Half-orientation extraction of palmprint features," Pattern Recognition Letters, vol. 69, pp. 35– 41, 2016.

[27] L. Fei, Y. Xu, W. Tang, and D. Zhang, "Double-orientation codeand nonlinear matching scheme for palmprint recognition," Pattern Recognition, vol. 49, pp. 89–101, 2016.

[28] R. Raghavendra, B. Dorizzi, A. Rao, and G. Hemantha Kumar, "Designing efficient fusion schemes for multimodal biometric systems using face and palmprint," Pattern Recognition, vol. 44, no. 5, pp. 1076–1088, 2011.

[29] S. C. Chen, H. G. Fu, and Y. Wang, "Application of improved graph theory image segmentation algorithm in tongue image segmentation," Computer Engineering and Applications, vol. 48, no. 5, pp. 201–203, 2012.

[30] El-Tarhouni, W., Boubchir, L., Elbendak, M., Bouridane, A. "Multispectral palmprint recognition using Pascal coefficients-based LBP and PHOG descriptors with random sampling," Neural Computing and Applications. 31, 593–603 (2019).

[31] Castro-Ortega, R., et al., "Zernike moment invariants for hand vein pattern description from raw biometric data," Journal of Electronic Imaging, 28(5), 053019 (2019).

[32] J. Gan and D. Zhou, "A Novel Method for Palmprint Recognition Based on Wavelet Transform," in Proceedings of the 2006 8th international Conference on Signal Processing, Guilin, China, November 2006.

[33] A. Giełczyk, M. Choraś, and R. Kozik, "Hybrid Feature Extraction for Palmprint-Based User Authentication", International Conference on High Performance Computing & Simulation (HPCS), pp. 629–633, 2018.

[34] X. Xu, Z. Guo, C. Song, and Y. Li, "Multispectral palmprint recognition using a quaternion matrix," Sensors, vol. 12, no. 4, pp. 4633–4647, 2012.

[35] Genovese A., Piuri V., Plataniotis K.N., Scotti F., "PalmNet: Gabor-PCA convolutional networks for touchless palmprint recognition," IEEE Transactions on Information Forensics and Security. 14 (2019) 3160–3174.

[36] J. P. Patil and C. S. Pawar, "Palmprint based Pattern Recognition Using Fast ICA," 2020 4th International Conference on Intelligent Computing and Control Systems (ICICCS), Madurai, India, 2020, pp. 566-569.

[37] J. Cui and Y. Xu, "Three dimensional palmprint recognition using linear discriminant analysis method," Innovations in Bio-inspired Computing and Applications, International Conference, pp. 107 111, 2011.

[38] G. Lu, D. Zhang, and K. Wang, "Palmprint recognition using eigenpalms features," Pattern Recognition Letters, vol. 24, no. 9- 10, pp. 1463–1467, 2003.

[39] F. Du, P. Yu, H. Li, and L. Zhu, "Palmprint recognition using gabor feature-based bidirectional 2dlda," Communications in Computer and Information Science, vol. 159, no. 2, pp. 230–235, 2011.

[40] W. El-Tarhouni, L. Boubchir, N. Al-Maadeed, M. Elbendak, and A. Bouridane, "Multispectral palmprint recognition based on local binary pattern histogram fourier features and gabor filter," in Proceedings of the 6th European Workshop on Visual Information Processing, EUVIP 2016, fra, October 2016.

[41] X. Xu, L. Lu, X. Zhang, H. Lu, and W. Deng, "Multispectral palmprint recognition using multiclass projection extreme learning machine and digital shearlet transform," Neural Computing and Applications, vol. 27, no. 1, pp. 143–153, 2016.

[42] C. Han, H. Cheng, C. Lin, and K. Fan, "Personal authentication using palm-print features," Pattern Recognition, vol. 36, no. 2, pp. 371–381, 2003.

[43] X. Wu, K. Wang, and D. Zhang, "HMMs Based Palmprint Identification," in Biometric Authentication, vol. 3072 of Lecture Notes in Computer Science, pp. 775–781, Springer Berlin Heidelberg, Berlin, Heidelberg, 2004.

[44] Mukherjee M., Meenpal T., Kinship verification using compound local binary pattern and local feature discriminant analysis, in: 2019 10th International Conference on Computing, Communication and Networking Technologies (ICCCNT), IEEE, 2019, pp. 1–7.

[45] Mohanty, F., Rup, S., Dash, B. (2018). An Improved CAD Framework for Digital Mammogram Classification Using Compound Local Binary Pattern and Chaotic Whale Optimization-Based Kernel Extreme Learning Machine. In: Kůrková, V., Manolopoulos, Y., Hammer, B., Iliadis, L., Maglogiannis, I. (eds) Artificial Neural Networks and Machine Learning – ICANN 2018. ICANN 2018. Lecture Notes in Computer Science(), vol 11140. Springer, Cham.

[46] http://biometrics.idealtest.org/dbDetailForUser.do?id=6.

[47] Faisal Ahmed, Emam Hossain, A.S.M. Hossain Bari and ASM Shihavuddin, "Compound Local Binary Pattern (CLBP) for Robust Facial Expression Recognition," IEEE International Symposium on Computational Intelligence and Informatics, pp.391-395, Budapest, Hungary, 2011.

[48] Wei Li, L. Zhang, D. Zhang and Jingqi Yan, "Principal line based ICP alignment for palmprint verification," *2009 16th IEEE International Conference on Image Processing (ICIP)*, 2009, pp. 1961-1964, doi: 10.1109/ICIP.2009.5413459.

[49] T. Ojala, M. Pietikainen and D. Harwood, A comparative study of texture measures with classification based on feature distributions, Pattern Recognition, vol. 29, 1996.

[50] Stan Z. Li, ChunShui Zhao, XiangXin Zhu, Zhen Lei, 2D+3D Face Recognition by Fusion at Both Feature and Decision Levels, In Proceedings of IEEE International Workshop on Analysis and Modeling of Faces and Ges-tures. Beijing. Oct 16, 2005.

[51] S. Koda, A. Zeggada, F. Melgani and R. Nishii, "Spatial and Structured SVM for Multilabel Image Classification," in *IEEE Transactions on Geoscience and Remote Sensing*, vol. 56, no. 10, pp. 5948-5960, Oct. 2018.

[52] Giannis Lantzanakis, Zina Mitraka, Nektarios Chrysoulakis, X-SVM: An Extension of C-SVM Algorithm for Classification of High-Resolution Satellite Imagery. IEEE Trans. Geosci. Remote. Sens. 59(5): 3805 3815 (2021).

[53] Q. Xiao, J. Lu, W. Jia and X. Liu, "Extracting Palmprint ROI From Whole Hand Image Using Straight Line Clusters," in *IEEE Access*, vol. 7, pp. 74327-74339, 2019.

[54] N. A. A. Khalid, M. I. Ahmad, T. H. Mandeel, M. N. M. Isa, R. A. R. Ahmad and M. Z. Nayef Al-Dabagh, "Palmprint ROI Cropping Based on Enhanced Correlation Coefficient Maximisation Algorithm," *2021 IEEE 11th International Conference on System Engineering and Technology (ICSET)*, 2021.

[55] Lu, Y Zhao, J Hu, "Enhanced Gabor-based region covariance matrices for palmprint recognition," IET Electronics letters, no. 17 : 880-881, 2009.

[56] Xu, Z Guo, C Song, Y Li, "Multispectral palmprint recognition using a quaternion matrix," Sensors 12, no. 4: 4633-4647, 2012.

[57] W Jia, RX Hu, YK Lei, Y Zhao and J. Gui. "Histogram of Oriented Lines for Palmprint Recognition," IEEE Transactions on Systems, Man, and Cybernetics: Systems, no. 3: 385-395, 2014.